# Crystal Structures of Zeolite Linde Type A Incorporating K Clusters: Dependence on the K Atom Loading Density

**T. Ikeda,*,† T. Kodaira,‡,§ F. Izumi,† T. Ikeshoji,|| and K. Oikawa⊥**

*Advanced Materials Laboratory, National Institute for Materials Science, 1−1 Namiki, Tsukuba, Ibaraki 305-0044, Japan, National Institute of Advanced Industrial Science and Technology, AIST Tsukuba central 5, Tsukuba, Ibaraki 305-8565, Japan, Structural Ordering and Physical Properties, PRESTO, Japan Science and Technology Corporation (JST), Japan, National Institute of Advanced Industrial Science and Technology, AIST Tsukuba central 2, Tsukuba, Ibaraki 305-8568, Japan, and Advanced Science Research Center, Japan Atomic Energy Research Institute, Tokai, Naka, Ibaraki 319-1195, Japan*

*Received: January 29, 2004*

Crystal structures of K-LTA (Linde Type A) incorporating K clusters of 0.35−6.4 K atoms per α-cage, which show ferromagnetism with the Curie temperature, $T_C$, up to 8 K, were determined by Rietveld analysis, followed by whole-pattern fitting on the basis of the maximum entropy method from X-ray and neutron powder diffraction data. Increasing the K content lowered space group symmetry without changing the double periodic ordering of α-cages. We identified space group $F\bar{4}3c$ in the low K content region. The $F\bar{4}3c$ model means that K clusters in adjacent α-cages must be equivalent to each other. Space group $F23$ in the high K content region leads to an alternate arrangement of two kinds of K clusters in neighboring α-cages. No structural phase transition occurred at $T_C$. The relationship between the crystal structure and ferromagnetism is discussed on the basis of the crystal data obtained in this work. The difference in the number of $K^+$ ions between the adjacent α-cages was estimated to be ca. 1.7 in K-loaded samples exhibiting ferromagnetism. Our results, coupled with magnetic data, support a spin-canting model of unpaired electrons in arrayed K clusters.

## 1. Introduction

Zeolites doped with alkali metals have aroused interest widely because of their physical properties, such as magnetism[1−5] and optical properties,[5−8] arising from alkali metal clusters accommodated in their cages. In these systems, *s* electrons of cationic alkali metal clusters formed from host cations and guest alkali metal atoms are localized in the cages. Magnetic properties of high-density clusters arrayed in zeolite cages are attractive in connection with various combinations of alkali metals and framework structures. Representative phenomena are the ferromagnetism of K clusters encapsulated in K ion-exchanged Linde Type A (K-LTA),[9] that of Rb clusters in Rb ion-exchanged LTA,[1,10] and the antiferromagnetism of Na clusters in sodalite.[4,11] Surprisingly, these compounds do not contain any magnetic elements. In the three systems, certain mutual interaction among neighboring clusters is believed to play important roles in the magnetic ordering.

Because of the alternative ordering of Si and Al atoms through O atom (i.e., Loewenstein's rule)[12] LTA with an ideal chemical composition of $Si_{96}Al_{96}O_{384}$ on its framework has a crystal structure with space group $Fm3c$ and a lattice parameter of $a \approx 24.6$ Å. LTA contains α- and β-cages possessing inner diameters of ca. 11 Å and ca. 7 Å, respectively. The number of K atoms, *n*, loaded per α-cage is controllable over a wide range up to 7.3 and strongly affects the magnetic properties of K-LTA incorporating the K clusters.[3] In what follows, this system will be abbreviated as $K_n$/K-LTA.

The origin of the magnetism in $K_n$/K-LTA has not yet been established. The largest spontaneous magnetization of $K_{5.2}$/K-LTA was only ca. 0.26 $\mu_B$ ($\mu_B$ = Bohr magneton) per K cluster at an applied external magnetic field of 100 Oe.[9] The magnetic structure of $K_n$/K-LTA is still unknown owing to difficulty in observing very weak magnetic scattering by neutron powder diffraction. The observation of no Drude term on the absorption spectra at $E > 0.3$ eV showed $K_n$/K-LTA to be a Mott insulator.[13,14] The K clusters in adjacent α-cages must interact antiferromagnetically, because the Weiss temperature $T_W$ yielded a negative value. Curie temperature, $T_C$, and $T_W$ strongly depend on the K loading density. At $n \approx 4$, $T_C$ and $T_W$ reached the maximum value of 8 K and the minimum value of ca. −40 K, respectively. Increasing *n* in a region of $n > 4$ lowered $T_C$ and raised $T_W$; both of them eventually approached 0 K at the maximum K content of $n = 7.2$.[15] A magnetization curve at 2 K did not saturate up to a magnetic field of 7 T, independent of *n* with no magnetic hysteresis observed except for a sample saturated with K.[13] Such magnetic behavior is suggestive of very soft magnetic ordering. Small saturation magnetization in an *n* region of $2 < n < 3$ and its continuous increase with an increase in *n* are incompatible with a model of ferrimagnetism.[15]

On the basis of these experimental facts, several models have been proposed for the magnetism of $K_n$/K-LTA. Nakano et al.[15] put forward a spin-canting model introducing the Dzyaloshisky−Moriya (DM) interaction[16−18] between magnetic moments of neighboring K clusters with a spin of $S = 1/2$. In the mass density wave model of Maniwa et al.,[19] two kinds of K clusters with $S = 0$ and 1 alternate with a super-exchange interaction

* Corresponding author. E-mail address: takuji-ikeda@aist.go.jp. Mailing address: National Institute of Advanced Industrial Science and Technology, AIST Tohoku, Nigatake 4−2−1, Miyagino-ku, Sendai, Miyagi 983-8551, Japan. Phone: +81-22-237-5211. Fax: +81-22-237-5226.

† National Institute for Materials Science.

‡ National Institute of Advanced Industrial Science and Technology.

§ Japan Science and Technology Corporation (JST).

|| National Institute of Advanced Industrial Science and Technology.

⊥ Japan Atomic Energy Research Institute.

10.1021/jp0400869 CCC: $27.50 
Published on Web 10/26/2004

among the K clusters with $S = 1$.[20] However, no structure−magnetism relationships have been explored from crystal and magnetic data in both studies.

A detailed crystallographic study is indispensable for understanding the mechanism of the ferromagnetism in $K_n$/K-LTA, because the magnetic ordering is closely associated with the atomic arrangement of the K clusters. We can acquire the knowledge of three-dimensional distribution of the K clusters from densities of electron and atomic nuclei (strictly speaking, coherent scattering length, $b_c$) in the unit cell of $K_n$/K-LTA.

Though Tao and Seff[21] and Armstrong et al.[22] reported the structures of $K_n$/K-LTA, neither of their samples showed ferromagnetism. Space groups $Pm\bar{3}m$ ($a \approx 12.3$ Å) and $Fm\bar{3}m$ ($a \approx 24.6$ Å) were adopted in the structural models of Tao and Seff and Armstrong et al., respectively. However, structural models derived from these two do not follow Loewenstein's rule that requires alternative ordering of Si and Al atoms through O atoms in the framework of LTA. Nishibori et al.[23] proposed another structural model adopting space group $F432$, which is a subgroup of $Fm\bar{3}m$ and satisfies Loewenstein's rule.

In previous works, we determined the crystal structures of $K_n$/K-LTA ($n = 4.0$, 5.0, and 5.2) by X-ray powder diffraction (XRD)[24] and time-of-flight neutron powder diffraction (TOF ND).[25] Space group $F\bar{2}3$ adopted by us has lower symmetry than $Fm\bar{3}m$ and $F432$. Reflections $hhl$ (e.g., 111 and 335) with a reflection condition of $h + l = 2m$ (even) appeared in our XRD patterns. These reflections, which were also observed by Maniwa et al.,[19] are inhibited in space group $Fm\bar{3}c$. The most important feature in our structural model is that K clusters in neighboring α-cages are nonequivalent to each other. The ordering of spins for K clusters must be closely related to the locations and numbers of $K^+$ ions in adjacent clusters. Whole-pattern fitting based on the maximum entropy method (MEM)[26,27] revealed the positional disorder of $K^+$ ions inside the α- and β-cages. No structural phase transition was observed at the measured temperature.[25]

The present study was undertaken to clarify the dependence of the distribution of $K^+$ ions on $n$ from angle-dispersive XRD and ND data. The complementary use of XRD and ND is very effective in analyzing the crystal structures of $K_n$/K-LTA unambiguously because of great differences in the relative scattering amplitudes of the constituent atoms between XRD and ND. Electron and nuclear densities have been visualized in three dimensions by our original technology of MEM-based pattern fitting (MPF)[28−30] in order to gain a better understanding of complex atomic configurations. The resulting electron and nuclear density maps directly offer information as to disordered atomic configurations. Including all the reflections with large lattice−plane spacings, $d$, in diffraction data is essential for the determination of nuclear densities by MEM. Unfortunately, the TOF ND data measured in our previous study[25] lacked eight reflections with large $d$ values. The large $d$ reflections are also indispensable for the determination of occupancies with sufficient accuracy.

In the present paper, we shall present structural data of $K_n$/K-LTA in a wide $n$ range from 0.35 to 6.4 and discuss the structure−property relationship in this system. The validity of our previous structural model[24,25] will be assessed from these crystal data. We will further point out an interesting relationship between local magnetic moments and differences in $n$ between adjacent α-cages.

## 2. Experimental Section

Na-type LTA (Na-LTA) was synthesized by us, with reference to previous reports.[31,32] To remove excessive $Na^+$ and $OH^-$ ions, the product was washed with deionized water. The resultant sample of Na-LTA had a cubic shape ca. 4 μm in average size. No impurities were detected in its XRD pattern. Na-LTA was converted into K-type LTA by soaking it three times in a 4 mol/dm$^3$ aqueous solution of KCl[2,3] and washed again with deionized water to remove excessive $K^+$ and $Cl^-$ ions. We gave attention to the LTA powder so it would not be protonated by the surplus washing. The chemical formula of K-LTA was determined as $K_{11.9}Si_{12.1}Al_{11.9}O_{48}$ per α-cage by using inductively coupled plasma (ICP) emission spectroscopy. Its Si/Al amount-of-substance ratio was 1.02. Na, Cl, and other impurity elements (e.g., Fe) could not be detected. There was a possibility that 0.1 $K^+$ ions per α-cage were exchanged into protons. Hereafter, we refer to this as K-LTA. K-LTA was dehydrated by heating it at 500 °C below $7 \times 10^{-4}$ Pa for 20 h in glass tubes. Without such exhaustive dehydration prior to the uptake of K atoms into K-LTA, residual water would have reacted with guest K atoms to decrease the number of 4s electrons included in the cages.

The dehydrated powder of K-LTA and distilled K metal in bulk were sealed in glass tubes in a glovebox filled with a high-purity He gas, whose oxygen and water contents were kept below 1 ppm to prevent the samples from their adsorption. The amounts of loaded K atoms per α-cage, $n$, were adjusted by changing the ratio of the mass of dehydrated K-LTA over that of distilled bulk K. K atoms were vaporized to be introduced into K-LTA by heating the tubes at 150 °C for 21 d, while repeating adsorption and homogenization with stirring many times to attain the most uniform distribution possible of K atoms loaded. $K_n$/K-LTA with $n = 0.35$, 2.8, 4.8, 4.9, 5.2, 5.8, and 6.4 were prepared in this way. The $n$ values were also confirmed by measuring diffuse reflection spectra of obtained samples and comparing spectral shapes and reflectivities with those reported previously.[2,13]

XRD data of the samples with $n = 0.35$, 2.8, 4.8, 5.2, and 6.4 were collected at room temperature on a MAC Science MXP-3TZ powder diffractometer. Its goniometer was equipped with a pair of long Soller slits to decrease the angular aperture to 1° and variable-width divergence and scattering slits to keep the sample irradiation width at 20 mm. Prior to the XRD experiments, the samples were placed in a detachable sample container in a glovebox filled with high-purity He gas, whose oxygen and water contents were kept below 1 ppm to prevent the samples from their adsorption. The sample container was transferred from the glovebox, set on the XRD goniometer, and evacuated. The pressure inside the container was kept below $5 \times 10^{-6}$ Pa during the XRD experiments. The XRD data were taken under the following conditions: Cu Kα radiation; operation voltage, 40 kV; tube current, 55 mA; scanning range, $4° \le 2\theta \le 100°$; step width, 0.016° in $4° \le 2\theta \le 38.5°$, 0.02° in $38.5° \le 2\theta \le 70°$, and 0.024° in $70° \le 2\theta \le 100°$; counting time per step, 100 s.

ND data of $K_n$/K-LTA with $n$ values of 4.9, 5.2, and 5.8 were measured at 7, 300, and 11 K, respectively, on the HRPD powder diffractometer at the JRR-3M reactor. Approximately 5 g of each sample was loaded into a cylindrical vanadium holder of 13 mm in diameter. Furthermore, this holder was placed in an aluminum vessel in the glovebox. The neutron wavelength, $\lambda$, was set at 1.824 Å using a Ge(331) monochromator with a takeoff angle of 89°. The scanning range was $4° \le 2\theta \le 160°$, and the step width was 0.05°.

Magnetization for $K_{5.2}$/K-LTA was measured in a temperature range from 2 to 300 K on a Quantum Design MPMS-XL SQUID magnetometer. Figure 1 shows magnetic moments, $M$'s,

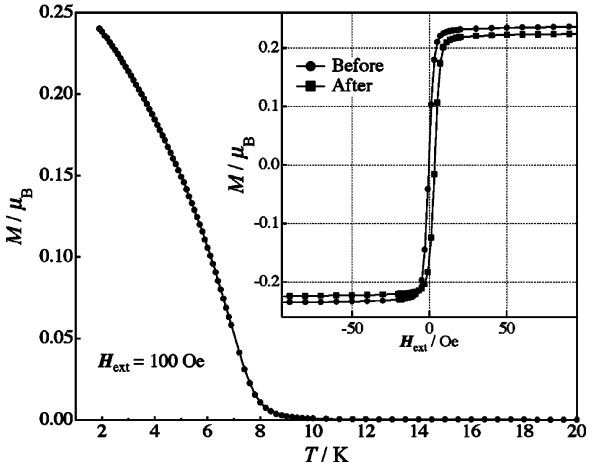


**Figure 1.** Dependence of the magnetic moment, $M$, per α-cage on temperature, $T$, in an external magnetic field strength, $\boldsymbol{H}_{ext}$, of 100 Oe (1 Oe = $[10^3/4\pi]$ A m$^{-1}$) for $K_4$/K-LTA. The inset shows a magnetization curve at 2 K before and after the XRD experiment of this sample.

per α-cage plotted against temperature, $T$; $M$ is the magnetization intensity divided by the amount of substance of $K_{5.2}$/K-LTA. $T_C$ was ca. 8 K. Values of $M$ before and after the XRD experiments remained virtually unchanged, as displayed in the inset of Figure 1. These magnetic data offer evidence that our samples exhibit ferromagnetism without any appreciable degradation during the XRD and ND measurements.[1,10,24,25] The most important point in our experiments is that the delicate samples are treated very carefully to not be degraded by the reaction of atmosphere.

### 3. Crystal Structures

**A. Possible Space Groups for K-LTA and $K_n$/K-LTA.** Pluth et al.[33] and Adams et al.[34] reported that dehydrated K-LTA crystallized in space group *Fm*3*c* with a lattice parameter of ca. $a \approx 24.6$ Å. On the other hand, our sample of K-LTA, dehydrated exhaustively, proved to be trigonal with space group $R\bar{3}c$, $R\bar{3}m$, *R*3*m*, *R*3*c*, or *R*32 and lattice parameters of $a = 24.5725(9)$ Å and $\alpha = 89.650(3)°$, in agreement with the crystal data reported in refs 25 and 35. The most probable space group is $R\bar{3}c$, the only maximal nonisomorphic subgroup of *Fm*3*c*. This discrepancy is ascribable to the inclusion of trace amounts of residual water in the cages of cubic K-LTA. In fact, we confirmed the reversibility of the trigonal−cubic change upon evacuation and exposure to air. Such a change in space group symmetry, accompanied by the adsorption and/or desorption of a guest, is often encountered with zeolites.

In $K_{0.35}$/K-LTA with $a = 24.5759(9)$ Å, reflection conditions derived from the indices of reflections observed unequivocally were $h + k$, $h + l$, $k + l = 2m$ (even) for *hkl*; $h$, $l = 2m$ for *hhl; k*, $l = 2m$ for 0*kl*; and $h = 2m$ for *h*00, which are consistent with cubic space groups $F\bar{4}3c$ (noncentrosymmetric) and *Fm*3*c* (centrosymmetric).

On the other hand, in $K_n$/K-LTA ($n \geq 2.8$) with $a$ between 24.656 and 24.707 Å, reflection conditions were $h + k$, $h + l$, $k + l = 2m$ for *hkl*; $h + l = 2m$ for *hhl; k*, $l = 2m$ for 0*kl*; and $h = 2m$ for *h*00 with *h*, *k*, *l* cyclically permutable, which affords possible space groups *F*23 (noncentrosymmetric) and *Fm*3 (centrosymmetric). Space groups *F*43*c*, *Fm*3*c*, *F*23, and *Fm*3 all lead to ordered arrangements of Si and Al atoms in conformity with Loewenstein's rule. Reflection conditions in the ND data of the three samples also agreed with those of space groups *F*23 and $Fm\bar{3}$ regardless of $n$ and temperatures. That is,

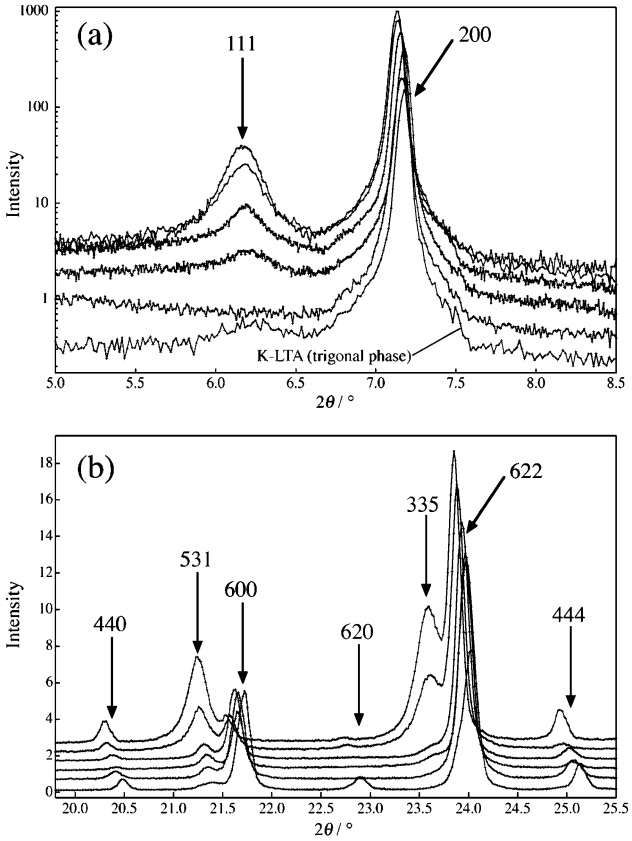


**Figure 2.** XRD data of $K_n$/K-LTA (part a) below $2\theta = 8.5°$ and (part b) in a region of $19.8° < 2\theta < 25.5°$. In both figures, $n = 0$, 2.8, 4.8, 5.2, and 6.5 from the bottom up.

neither phase transition nor appreciable structural changes were observed in our ND experiments. XRD intensities of reflections whose reflection conditions are $h$, $k$, $l = 2m + 1$ (odd) (e.g., 111, 531 and 335) remarkably increased with increasing $n$, as Figure 2 illustrates. Profiles of these reflections were appreciably broadened in comparison with those of the other reflections.

In the present system, crystal symmetry can be narrowed down but cannot be determined uniquely from reflection conditions obtained using powder diffraction data. Therefore, the validity of possible structural models needs artful structural refinements as will be described.

**B. Procedures of Rietveld Refinements and MPF.** All of the intensity data were first analyzed by the Rietveld method with RIETAN-2000.[28−30] An isotropic atomic displacement parameter, $U$, was assigned to each site, with the isotropic Debye−Waller factor defined as $\exp(-8\pi^2 U \sin^2\theta/\lambda^2)$. Coefficients for the analytical approximation to atomic scattering factors for $Si^{4+}$, $Al^{3+}$, and $K^+$ were taken from ref 36 and those for $O^{2-}$ from ref 37. Values of $b_c$ used for the Rietveld refinements of the ND data were 3.449 fm (Si), 4.149 fm (Al), 5.803 fm (O), and 3.710 fm (K).[36] Occupancies, $g$'s, of Al and Si sites were fixed so as to give the Si/Al amount-of-substance ratio of 1.02. The split pseudo-Voigt function of Toraya[38] was used as a profile function. Partial profile relaxation with a modified split pseudo-Voigt function[39] was applied to parts of (nearly) isolated reflections with anisotropic broadening and/or highly asymmetric profiles in the low $2\theta$ region, which dramatically improved fits between their observed and calculated profiles. An 11th-order Legendre polynomial was fit to the background.

Disordered atomic arrangements, characteristic of guests taken up in zeolite frameworks, can adequately be represented by

electron/nuclear density distribution determined by MEM. At first, observed structure factors, $F_o$'s (Rietveld), are evaluated after Rietveld analysis to a first approximation. To estimate $F_o$ (Rietveld), the observed diffraction intensity at each point is apportioned in the ratio of profiles calculated from final parameters refined by the Rietveld method and summed up for each reflection.[40] Electron/nuclear densities are determined by MEM from the $F_o$ (Rietveld) values. In this work, MEM analyses were carried out using MEED[41] on an SGI Origin 2000 parallel computer. The spatial resolution was 256 × 256 × 256 pixels per unit cell. MEM is, per se, model-free, and can provide values of isolated reflections consistent with a good model, that is, a good guess. Hence, the resulting electron/nuclear densities more or less reflect contributions of structural details neglected in the Rietveld analysis.[26,27]

After the first MEM analysis, electron/nuclear density distribution is redetermined by MPF,[28−30] which is the structure refinement utilizing the combination of whole-pattern fitting (RIETAN-2000) and MEM analysis (MEED). MEM analyses and whole-pattern fitting are alternately repeated (REMEDY cycles) until *R* factors in the latter no longer decrease. In the present study, structural models were revised by the full examination of density maps, if necessary. Modifications of structural models were repeated until a revised structural model agreed well with the density maps resulting from the iterative procedure just described.[42−44]

The 4s electrons are considerably delocalized in the α- and β-cages, and a small amount of 4s electrons do not contribute to XRD intensities appreciably. The 4s electrons, therefore, cannot directly be observed by the MPF structure refinement from the XRD data. Nevertheless, the most probable electron densities determined by MPF provide us with detailed information on chemical bonding and localized electrons. The MPF structure refinement from the ND data containing negligible contributions of electrons is particularly suitable for learning the distribution of disordered atoms.

**C. Structure Refinement of $K_{0.35}$/K-LTA.** We searched for $K^+$ ions loaded into $K_n$/K-LTA in electron density maps plotted after MPF by comparing them with the positions of $K^+$ ions in dehydrated K-LTA.[34,45] Sites for $K^+$ ions loaded were neglected in an initial structural model adopting space group $Fm\bar{3}c$ in the Rietveld analysis of $K_{0.35}$/K-LTA. Most positions of $K^+$ ions proved to be close to four-, six-, and eight-membered rings. A $K^+$ site at 64*e* (*x*, *x*, *x*; $x \approx 0.12$) in the six-membered ring shared by α- and β-cages had an extraordinarily large *U* parameter of ca. 11 nm$^2$. This finding promoted us to split this K site into two pieces: One was displaced toward the center of the β-cage, while the other was located near the plane of the six-membered ring perpendicular to the [111] axis. The sum of refined occupancies for the two split sites was as large as 1.24. The space group symmetry of $Fm\bar{3}c$ is, therefore, too high to gain a reasonable arrangement of $K^+$ ions in $K_{0.35}$/K-LTA.

Next, we adopted another structural model derived from $F\bar{4}3c$, which is a subgroup of $Fm\bar{3}c$. A K site at 32*e* (*x*, *x*, *x*; $x \approx 0.12$) in the six-membered ring was split into four sites K1a, K1b, K2a, and K2b. In this model, the sum of *g*(K1a) and *g*(K1b), and *g*(K2a) and *g*(K2b) were close to unity. Therefore, their occupancies were constrained, hereafter, so as to satisfy the simple relations of *g*(K2a) = *g*(K1a) and *g*(K1b) = *g*(K2b) = 1 − *g*(K1a). Regular tetrahedral assemblies of the four K2a sites were recognized in the β-cage, with a K2a−K2a distance, *l*(K2a−K2a), of ca. 4.13 Å. Examining electron density maps resulting from MPF, we found an additional K3 site with a small occupancy in the α-cage and a K4 site at 96*h* (*x*, *y*, *z*) beside the four-membered ring and inside the α-cage. A K site that had been first located at 24*c* (0, 1/4, 1/4) near the center of an eight-membered ring was split into two sites, K5 at 24*c* and K6 at 96*h*, because electron densities due to positional disorder were detected at these positions in electron density maps plotted after MPF. Therefore, we decided the space group of $K_{0.35}$/K-LTA is $F\bar{4}3c$ with a slightly disordered distribution of $K^+$ ions.

**D. Structure Refinements of $K_n$/K-LTA ($n \geq 2.8$).** Reflection conditions of $Fm\bar{3}$ are just the same as those of *F*23. *F*23 is a subgroup of $F\bar{4}3c$, while $Fm\bar{3}$ is a subgroup of not $F\bar{4}3c$ but $Fm\bar{3}c$. The space group of $K_n$/K-LTA ($n \geq 2.8$) is expected to be a subgroup of $F\bar{4}3c$, adopted for $K_{0.35}$/K-LTA. In the $Fm\bar{3}$ model, the structural parameters could not converged, which indicates that a nonequivalence K cluster in adjacent α-cages cannot be considered, because all local symmetry for the $K^+$ ion gives an equivalent atom position between the neighboring α-cages. Accordingly, we analyzed the intensity data of $K_n$/K-LTA with $n > 0.35$ on the basis of space group *F*23.[25]

Two pairs of split 16*e* (*x*, *x*, *x*) sites for K atoms were found near the center of each six-membered ring in the Rietveld analysis: K1a−K1b and K2a−K2b. Sites K1a, K1b, K2a, and K2b were distributed beside the six-membered rings of the β-cage. Site K1a was situated in the β-cage, while the other three sites outside the β-cage (viz., inside the neighboring α-cage). K1c and K2c sites near two different six-membered rings in another β-cage were located inside and outside the β-cage, respectively. In $K_{6.4}$/K-LTA (XRD) at room temperature and $K_{4.9}$/K-LTA (ND) at 11 K, sites K1c and K2c were further split to add sites K1d and K2d, respectively, considering rather large estimated standard deviations of their fractional coordinates and *U* values.

The sum of occupancies for $K^+$ ions in each six-membered ring was approximately equal to unity. Hence, *g*(K2a), *g*(K1b), and *g*(K2b) were constrained in such a way that *g*(K2a) = *g*(K1a) and *g*(K1b) = *g*(K2b) = 1 − *g*(K1a). Occupancies *g*(K1d) and *g*(K2d) were also constrained in a similar manner: *g*(K1d) = *g*(K2d) = 1 − *g*(K1c). The possibility of simultaneous occupation of the two K positions (viz., one in the α-cage and the other in the β-cage) close to the same six-membered ring was excluded in consideration of strong electrostatic repulsion between the two $K^+$ ions.

Sites K3a and K3b displaced off the center of the four-membered ring were assigned to $K^+$ ions near this ring. These two were included in α-cages neighboring each other. The difference between *g*(K3a) and *g*(K3b) increased with increasing *n*. Site K4 lay beside the center of the α-cage including the K3b site. Two $K^+$ ions distributed statistically between sites K5 and K6 were detected by MPF near the center of the eight-membered ring. Site K5 was located at a 24*g* site (*x*, 1/4, 1/4; $x \approx 0$). Site K6 shifted slightly from the center of the eight-membered ring to the α-cage accommodating the K4 site. The sum of *g*(K5) and *g*(K6) was approximately equal to unity regardless of *n*. Such an arrangement of $K^+$ ions is in accord with the view that $K_n$/K-LTA is essentially inhomogeneous with regard to the distribution of $K^+$ ions.

In final Rietveld refinements, all the *U* parameters for Si and Al sites were constrained to be equal to each other: *U*(Si1) = *U*(Si2) = *U*(Al1) = *U*(Al2). Simple approximations *U*(K1a) = *U*(K1b) = *U*(K1c) = *U*(K2a) = *U*(K2b) = *U*(K2c) = *U*(K1d) = *U*(K2d), *U*(K3a) = *U*(K3b), and *U*(K5) = *U*(K6) were also imposed on the *U* parameters of the K sites near the six-, four- and eight-membered rings, respectively.

Structure parameters refined by the Rietveld method from the ND data were in good agreement with those determined

from the XRD data. Fractional coordinates of all the $K^+$ ions for $K_n$/K-LTA with $n = 4.9$, 5.2, and 5.8 were almost the same as those refined for $K_{5.2}$/K-LTA from its XRD data. Structural changes with decreasing temperature were subtle. Occupancies of all K sites have no change. All of the K sites in the six-membered ring shifted a little along the [111] axis. The K4 site was somewhat displaced toward the center of the α-cage. The other K sites were displaced only slightly by raising the temperature. In the cases of the ND data for $K_{4.9}$/K-LTA at 11 K and $K_{5.8}$/K-LTA at 7 K, the K5 and K6 sites concentrated near the center of the eight-membered ring.

**E. Results of the Structure Refinements.** Rietveld refinements based on the structural model described already gave fairly good fits between the observed and calculated intensities. Table 1 summarizes *R* factors and lattice and structure parameters obtained for all the samples of $K_n$/K-LTA by the Rietveld refinements from both the XRD and ND data. Values of *n* calculated from the *g*(K)'s refined in the Rietveld analyses agreed well with those estimated from the optical spectra. Figure 3 gives the dependence of the lattice parameter, *a*, refined from the XRD data taken at room temperature on *n*, together with lattice parameters refined from the ND data ($n = 4.9$ at 11 K and $n = 5.8$ at 7 K) and TOF ND data ($n = 4.0$ at 4.5 K).[25] The lattice parameter at room temperature increased monotonically with increasing *n*. In the low-temperature ND experiments, the maximum *a* parameter of 24.6578(5) Å was obtained for $K_{4.9}$/K-LTA at 11 K. To discuss structural changes accompanying the introduction of K atoms, we will also refer to the results of the TOF ND study from now on.

Table 1 shows that *R* factors attached with the primes were considerably lowerafter REMEDY cycles in all samples of $K_n$/K-LTA. Striking decreases in $R_B$ and $R_F$ evaluated from observed integrated intensities[40] are particularly noteworthy. Observed, calculated, and difference patterns for the XRD data of $K_{6.4}$/K-LTA and the ND data of $K_{5.8}$/K-LTA at 7 K are plotted against $2\theta$ in Figure 4.

Electron densities determined by MPF for the samples with $n = 2.8$, 5.2, and 6.5 were summed up in a *z* range of $0.21 < z < 0.29$ parallel to the *c* axis and projected onto the (001) plane (Figure 5a). Nonequivalent and disordered arrangements of $K^+$ ions in adjacent α-cages are clearly visible. Here, one α-cage including the K3b and K4 sites will be referred to as α-cage A and the other α-cage including the K3a site as α-cage B. Figure 5b displays corresponding electron density maps of the (110) planes. Electron densities of $K^+$ ions elongated along the [111] axis can be seen in the six-membered ring. Our structural model yielded a pair of regular tetrahedral assemblies of $K^+$ ions (i.e., the K1a and the K2c sites in adjacent *β*-cages). However, no electron densities due to chemical bonding were detected between any two $K^+$ ions in the tetrahedral assemblies. Nuclear density maps plotted in a similar manner (Figure 6) were in accord with the electron density maps displayed in Figure 5.

Figure 7 illustrates a structural drawing of $K_{5.2}$/K-LTA where partial occupation of $K^+$ ions is neglected for convenience. Unless otherwise noted, we shall mainly concern ourselves with discussing the structure of $K_{5.2}$/K-LTA with the largest spontaneous magnetization, because the other samples of $K_n$/K-LTA bear a marked structural resemblance to $K_{5.2}$/K-LTA.

## 4. Structure−Magnetism Relationship in the $K_n$/K-LTA System

**A. Comparison with the Other Structural Models.** The three other structural models adopting space groups $Pm\bar{3}m$,[21] $Fm\bar{3}m$,[22] and $F432$[23] have hitherto been proposed for $K_n$/K-LTA ($n \geq 2.8$). In the structural studies of Tao and Seff[21] and Armstrong et al.,[22] the temperatures of dehydrating K-LTA and incorporating K atoms seem to be too low and too high, respectively. Insufficient dehydration leads to the inclusion of a trace amount of residual $H_2O$ molecules in the *β*-cages;[31] they readily react with K atoms loaded. The uptake of K atoms into K-LTA at the high temperatures will destroy part of framework. Their samples most probably underwent such chemical reactions and structural degradation, which may be the reason their samples did not exhibit ferromagnetism.[21,22]

The $Pm\bar{3}m$ model is inconsistent with the reflection conditions derived from our diffraction data. In the $Fm\bar{3}m$ model, the numbers of $K^+$ ions in adjacent α-cages differ from each other in the analogy with our $F23$ model. A $K_{12}^{4+}$ cluster composed of $K^+$ ions beside four-membered rings is situated in one α-cage, whereas $K^+$ cations are located only in the six-membered rings in the other α-cage.[22] The *n* value was calculated at 4.87 from the *g*(K)'s refined from our XRD data of $K_{5.2}$/K-LTA with the $Fm\bar{3}m$ model. It is smaller than the *n* value of 5.2 estimated from the diffuse reflection spectra. This difference between the *n* values determined from *g*(K)'s and the reflection spectra increased from 0.3 to 0.6 when increasing *n* from 2.8 to 6.4. Final $R_{wp}$ values obtained with the $Fm\bar{3}m$ model were also 5−7% larger than those resulting from the $F23$ model. Thus, our experimental and refinement results reject the possibilities of the $Pm\bar{3}m$ and $Fm\bar{3}m$ models.

The $F432$ model put forward by Nishibori et al.[23] permits the alternate ordering of the Si and Al sites. In their model, locations of $K^+$ ions are similar to those in the $Fm\bar{3}m$ model, but we detected an additional K site near the center of an α-cage including the $K_{12}^{4+}$ cluster in electron density maps obtained by the MPF on the basis of the $F432$ model. However, its occupancies, refined from the XRD and ND data by adopting this model, appreciably differed from each other despite its comparable fractional coordinates. In $K_{5.2}$/K-LTA, the *g*(K) value of a 48*h* site ($1/2\ y, y; y \approx 0.375$) near the four-membered ring was estimated at 0.854 from the XRD data but at 0.531 from the ND data.

Space groups $Fm\bar{3}m$ and $F432$ have the same reflection conditions. Origins in the $Fm\bar{3}m$ and $F432$ models were different from those in the $Fm\bar{3}c$, $F\bar{4}3c$, and $F23$ models. With these two models, the total numbers of $K^+$ ions per unit cell were somewhat less than those determined from the reflection spectra. Differences in the number of K atoms between adjacent α-cages were unreasonably large. For example, the difference amounted to 10.3 in the Rietveld analysis of $K_{5.2}$/K-LTA with the $F432$ model. $K^+$ ions should occupy positions near the four-membered ring in each α-cage to neutralize the negative charge on the framework, which is, however, not achieved in the $Fm\bar{3}m$ or $F432$ models.

In conclusion, our results of the structure refinements from both the XRD and ND data of the high-quality samples deny the validity of the $Pm\bar{3}m$,[21] $Fm\bar{3}m$,[22] and $F432$[23] models.

**B. Stability of the K Clusters in the *β*-Cage.** Alkali metal clusters in *β*-cages have been investigated with regard to their locations and conformations in previous work.[21,22,46−49] Ursenbach et al.[49] predicted the existence of $Na_4^{3+}$ clusters in *β*-cages of Na-type Faujasite, Na-FAU(Y), with amount-of-substance ratios, Si/Al, greater than 1.5 by Car−Parrinello molecular dynamics. $K_3^{2+}$ clusters incorporated into *β*-cages in K-FAU(X) with an Si/Al ratio smaller than 1.5 were observed in an electron spin resonance (ESR) spectrum of a sample doped with a small amount of K.[50] $K_4^{3+}$ clusters in *β*-cages of K-FAU(Y)

**TABLE 1: Crystal Data of $K_n$/K-LTA ($Si_{96.96}Al_{95.04}O_{384}K_{96+8n}$) Obtained by the Rietveld Refinements[a]**

| | | | | | | | | | |
|---|---|---|---|---|---|---|---|---|---|
| *n* | | 0.35 | 2.8 | 4.8 | 5.2 | 6.4 | 4.9 | 5.2 | 5.8 |
| *T* | | room temperature | room temperature | room temperature | room temperature | room temperature | 11 K | room temperature | 7 K |
| diffraction | | XRD | XRD | XRD | XRD | XRD | ND | ND | ND |
| space group | | $F\bar{4}3c$ | $F23$ | $F23$ | $F23$ | $F23$ | $F23$ | $F23$ | $F23$ |
| $R_{wp}/R_p/R_e$ (%) | | 5.63/3.55/ 5.79 | 7.27/4.19/ 8.38 | 7.69/4.55/ 6.43 | 8.25/5.35/ 7.61 | 8.68/5.65/ 7.89 | 5.23/4.03/ 3.36 | 5.61/4.39/ 4.59 | 4.93/3.77/ 3.30 |
| $R'_{wp}/R'_p$ (%) | | 5.48/3.49 | 6.76/3.81 | 6.85/3.71 | 7.30/4.56 | 8.04/5.29 | 5.07/3.87 | 3.24/1.66 | 4.85/3.66 |
| $R_B/R_F$ (%) | | 1.18/0.94 | 2.85/2.44 | 2.70/2.06 | 2.68/1.68 | 2.72/1.94 | 1.83/0.86 | 3.24/1.66 | 1.38/0.66 |
| $R'_B/R'_F$ (%) | | 1.11/0.86 | 1.67/1.72 | 1.63/1.02 | 1.30/1.06 | 2.60/1.36 | 1.46/0.68 | 3.24/1.66 | 1.29/0.61 |
| Lattice constant: *a* | | 24.5759(9) | 24.6131(6) | 24.6595(9) | 24.6685(4) | 24.7065(9) | 24.6578(5) | 24.6634(5) | 24.6573(3) |
| Si1 | *x* | −0.0016(4) | −0.0011(11) | 0.0011(7) | −0.0047(11) | −0.0014(7) | 0.000(2) | −0.002(3) | 0.0014(11) |
| 48*h* | *y* | 0.0917(4) | 0.0974(8) | 0.0905(8) | 0.0932(9) | 0.0926(8) | 0.0947(9) | 0.093(3) | 0.0947(9) |
| 96*h*[b] | *z* | 0.1867(4) | 0.1905(9) | 0.1840(7) | 0.1878(8) | 0.1892(8) | 0.1879(10) | 0.188(3) | 0.1893(8) |
| | $U$/nm$^2$ | 1.90(8) | 0.99(11) | 0.89(10) | 1.48(11) | 1.39(13) | 0.39(8) | 1.32(14) | 0.34(4) |
| Si2 | | $g = 0.01$, $x = x$(Al), $y = y$(Al), $z = z$(Al), and $U = U$(Si1) for all data | | | | | | | |
| Al | *g* | 0.99 | 0.99 | 0.99 | 0.99 | 0.99 | 0.99 | 0.99 | 0.99 |
| 48*h* | *x* | 0.0024(4) | 0.0006(9) | −0.0015(8) | −0.0004(11) | −0.0001(9) | 0.000(2) | 0.002(3) | 0.0013(13) |
| 96*h*[b] | *y* | 0.1881(4) | 0.1863(8) | 0.1911(8) | 0.1930(9) | 0.1899(8) | 0.1929(8) | 0.188(4) | 0.1901(9) |
| | *z* | 0.0932(4) | 0.0899(8) | 0.0976 (8) | 0.0925(9) | 0.0928(8) | 0.0887(7) | 0.091(4) | 0.0904(8) |
| | $U$/nm$^2$ | = $U$(Si1) | = $U$(Si1) | = $U$(Si1) | = $U$(Si1) | = $U$(Si1) | = $U$(Si1) | = $U$(Si1) | = $U$(Si1) |
| Si1b | *x* | | 0.5899(8) | 0.5945(7) | 0.5911(11) | 0.5910(9) | 0.5939(9) | 0.594(3) | 0.5933(8) |
| 48*h* | *y* | | 0.5021(9) | 0.4975(8) | 0.5004(11) | 0.5030(8) | 0.502(2) | 0.502(3) | 0.5007(10) |
| | *z* | | 0.6801(8) | 0.6857(8) | 0.6863(9) | 0.6893(7) | 0.6879(11) | 0.689(3) | 0.6864(8) |
| | $U$/nm$^2$ | | = $U$(Si1) | = $U$(Si1) | = $U$(Si1) | = $U$(Si1) | = $U$(Si1) | = $U$(Si1) | = $U$(Si1) |
| Si2b | | | | $g = 0.01$, $x = x$(Alb), $y = y$(Alb), $z = z$(Alb), and $U = U$(Si1) except $K_{0.35}$/K-LTA | | | | | |
| Alb | *g* | | 0.99 | 0.99 | 0.99 | 0.99 | 0.99 | 0.99 | 0.99 |
| 48*h* | *x* | | 0.6855(9) | 0.6816(8) | 0.6815(9) | 0.6825(7) | 0.6881(9) | 0.688(3) | 0.6917(9) |
| | *y* | | 0.4992(12) | 0.5036(7) | 0.4962(11) | 0.4947(7) | 0.501(2) | 0.503(4) | 0.5036(11) |
| | *z* | | 0.5950(9) | 0.5895(8) | 0.5918(10) | 0.5904(8) | 0.5951(11) | 0.592(3) | 0.5957(9) |
| | $U$/nm$^2$ | | = $U$(Si1) | = $U$(Si1) | = $U$(Si1) | = $U$(Si1) | = $U$(Si1) | = $U$(Si1) | = $U$(Si1) |
| O1 | *x* | 0.0028(10) | −0.0043(13) | 0.0034(12) | 0.00(2) | 0.000(11) | 0.0061(6) | 0.0061(13) | 0.0063(5) |
| 48*h* | *y* | 0.1208(2) | 0.1280(7) | 0.1103(5) | 0.1211(14) | 0.1212(9) | 0.1230(6) | 0.121(2) | 0.1235(6) |
| 96*h*[b] | *z* | 0.2447(7) | 0.2578(11) | 0.2520(12) | 0.254(2) | 0.2576(11) | 0.2473(7) | 0.2486(14) | 0.2473(6) |
| | $U$/nm$^2$ | 2.0(3) | 2.3(4) | 3.2(3) | 1.8(4) | 2.0(3) | 0.96(10) | 2.2(3) | 1.03 (9) |
| O2 | *x* | 0.0002(7) | −0.0028(13) | −0.0014(13) | −0.0073(8) | −0.0059(9) | −0.0056(4) | −0.0072(6) | −0.0072(6) |
| 48*h* | *y* | 0.1406(5) | 0.1410(9) | 0.1434(9) | 0.146(2) | 0.1419(11) | 0.1384(7) | 0.144(2) | 0.1374(6) |
| 96*h*[b] | *z* | 0.1458(5) | 0.1450(10) | 0.1396(9) | 0.144(2) | 0.1415(11) | 0.1389(7) | 0.145(2) | 0.1393(6) |
| | $U$/nm$^2$ | 1.1(3) | 2.4(4) | 3.0(4) | 2.0(4) | 2.2(4) | 0.71(8) | 1.6(2) | 0.67(9) |
| O3 | *x* | 0.5560(6) | 0.5520(11) | 0.5558(9) | 0.5562(13) | 0.5632(11) | 0.5564(9) | 0.556(2) | 0.5545(6) |
| 48*h* | *y* | 0.5556(6) | 0.5552(12) | 0.5500(9) | 0.5547(14) | 0.5534(11) | 0.5543(9) | 0.554(2) | 0.5543(6) |
| 96*h*[b] | *z* | 0.3178(3) | 0.3292(11) | 0.3308(9) | 0.3370(7) | 0.3249(8) | 0.3233(5) | 0.3220(10) | 0.3223(5) |
| | $U$/nm$^2$ | 1.4(3) | 3.3(6) | 3.2(5) | 3.2(5) | 2.8(4) | 0.72(3) | 1.4(2) | 0.4(2) |
| O4 | *x* | 0.5580(7) | 0.5564(11) | 0.5629(11) | 0.557(2) | 0.5481(9) | 0.5562(8) | 0.5561(6) | 0.5561(6) |
| 48*h* | *y* | 0.5614(7) | 0.5647(11) | 0.5564(11) | 0.560(2) | 0.5517(8) | 0.5605(10) | 0.5624(7) | 0.5624(7) |
| 96*h*[b] | *z* | 0.1703(4) | 0.1774(10) | 0.1840(9) | 0.1778(8) | 0.1659(7) | 0.1785(5) | 0.1772(5) | 0.1772(5) |
| | $U$/nm$^2$ | 2.9(3) | 2.0(4) | 2.4(4) | 2.7(4) | 2.4(5) | 1.3(3) | 1.4(3) | 1.4(3) |
| O1b | *x* | | 0.6069(6) | 0.6296(7) | 0.6200(14) | 0.6178(10) | 0.6255(6) | 0.622(2) | 0.6250(6) |
| 48*h* | *y* | | 0.4937(10) | 0.5054(13) | 0.499(2) | 0.5015(14) | 0.4970(7) | 0.498(2) | 0.4975(6) |
| | *z* | | 0.7404(9) | 0.7365(9) | 0.5918(10) | 0.7432(11) | 0.7477(7) | 0.7482(11) | 0.7482(7) |
| | $U$/nm$^2$ | | = $U$(O1) | = $U$(O1) | = $U$(O1) | = $U$(O1) | = $U$(O1) | = $U$(O1) | = $U$(O1) |
| O2b | *x* | | 0.6402(10) | 0.6319(10) | 0.635(2) | 0.6361(13) | 0.6417(6) | 0.640(2) | 0.6417(6) |
| 48*h* | *y* | | 0.5030(15) | 0.5043(14) | 0.5045(11) | 0.5144(8) | 0.5511(5) | 0.4997(9) | 0.5006(5) |
| | *z* | | 0.6395(10) | 0.6396(9) | 0.742(2) | 0.6403(13) | 0.6431(6) | 0.641(2) | 0.6428(6) |
| | $U$/nm$^2$ | | = $U$(O2) | = $U$(O2) | = $U$(O2) | = $U$(O2) | = $U$(O2) | = $U$(O2) | = $U$(O2) |
| O3b | *x* | | 0.0487(10) | 0.0568(9) | 0.058(2) | 0.0642(9) | 0.0524(8) | 0.055(2) | 0.0534(6) |
| 48*h* | *y* | | 0.0570(11) | 0.0488(9) | 0.057(2) | 0.0589(11) | 0.0552(9) | 0.056(2) | 0.0568(7) |
| | *z* | | 0.8199(12) | 0.8212(10) | 0.8128(9) | 0.8036(7) | 0.8160(5) | 0.8164(9) | 0.8153(4) |
| | $U$/nm$^2$ | | = $U$(O3) | = $U$(O3) | = $U$(O3) | = $U$(O3) | = $U$(O3) | = $U$(O3) | = $U$(O3) |
| O4b | *x* | | 0.0580(10) | 0.0681(10) | 0.063(2) | 0.0560(14) | 0.0599(8) | 0.058(2) | 0.0583(8) |
| 48*h* | *y* | | 0.0648(11) | 0.0563(9) | 0.059(2) | 0.0581(14) | 0.0562(8) | 0.055(2) | 0.0561(8) |
| | *z* | | 0.6801(9) | 0.6840(11) | 0.6862(9) | 0.6814(7) | 0.6843(5) | 0.6788(9) | 0.6849(4) |
| | $U$/nm$^2$ | | = $U$(O4) | = $U$(O4) | = $U$(O4) | = $U$(O4) | = $U$(O4) | = $U$(O4) | = $U$(O4) |
| K1a | *g* | 0.670(4) | 0.236(5) | 0.221(6) | 0.616(7) | 0.795(7) | 0.81(2) | 0.56(6) | 0.60(12) |
| 16*e* | *x* | 0.1083(2) | 0.0546(11) | 0.0481(9) | 0.0640(6) | 0.0711(5) | 0.0704(9) | 0.061(2) | 0.066(2) |
| 32*e*[b] | *y* | = *x* | = *x* | = *x* | = *x* | = *x* | = *x* | = *x* | = *x* |
| | *z* | = *x* | = *x* | = *x* | = *x* | = *x* | = *x* | = *x* | = *x* |
| | $U$/nm$^2$ | 1.25 (11) | 4.8(3) | 4.9(3) | 2.9(2) | 2.5(3) | 0.8(3) | 2.2(4) | 0.5(3) |

**TABLE 1 (Continued)**

| | | | | | | | | | |
|---|---|---|---|---|---|---|---|---|---|
| K1b | *g* | = 1 − *g*(K1a) | = 1 − *g*(K1a) | = 1 − *g*(K1a) | = 1 − *g*(K1a) | = 1 − *g*(K1a) | = 1 − *g*(K1a) | 1 − *g*(K1a) | = 1 − *g*(K1a) |
| 16*e* | *x* | 0.1306(4) | 0.1199(6) | 0.1149(6) | 0.1188(9) | 0.10811(13) | 0.113(4) | 0.111(2) | 0.078(2) |
| 32*e*[b] | *y* | = *x* | = *x* | = *x* | = *x* | = *x* | = *x* | = *x* | = *x* |
| | *z* | = *x* | = *x* | = *x* | = *x* | = *x* | = *x* | = *x* | = *x* |
| | *U*/nm$^2$ | = *U*(K1a) | = *U*(K1a) | = *U*(K1a) | = *U*(K1a) | = *U*(K1a) | = *U*(K1a) | = *U*(K1a) | = *U*(K1a) |
| K1c | *g* | | 1 | 1 | 1 | 0.285(4) | 0.21(6) | 1 | 1 |
| 16*e* | *x* | | 0.6228(7) | 0.6210(5) | 0.6174(4) | 0.5997(12) | 0.6310(3) | 0.6263(13) | 0.6136(8) |
| | *y* | | = *x* | = *x* | = *x* | = *x* | = *x* | = *x* | = *x* |
| | *z* | | = *x* | = *x* | = *x* | = *x* | = *x* | = *x* | = *x* |
| | *U*/nm$^2$ | | = *U*(K1a) | = *U*(K1a) | = *U*(K1a) | = *U*(K1a) | = *U*(K1a) | = *U*(K1a) | = *U*(K1a) |
| K1d | *g* | | | | | = 1 − *g*(K1c) | = 1 − *g*(K1c) | | |
| 16*e* | *x* | | | | | 0.6209(9) | 0.6146(14) | | |
| | *y* | | | | | = *x* | = *x* | | |
| | *z* | | | | | = *x* | = *x* | | |
| | *U*/nm$^2$ | | | | | = *U*(K1a) | = *U*(K1a) | | |
| K2a | *g* | = *g*(K1a) | = *g*(K1a) | = *g*(K1a) | = *g*(K1a) | = *g*(K1a) | = *g*(K1a) | = *g*(K1a) | = *g*(K1a) |
| 16*e* | *x* | −0.1209(2) | −0.069(2) | −0.075(2) | −0.1300(4) | −0.1199(5) | −0.1166(13) | −0.124(2) | −0.116(2) |
| 32*e*[b] | *y* | = *x* | = *x* | = *x* | = *x* | = *x* | = *x* | = *x* | = *x* |
| | *z* | = *x* | = *x* | = *x* | = *x* | = *x* | = *x* | = *x* | = *x* |
| | *U*/nm$^2$ | = *U*(K1a) | = *U*(K1a) | = *U*(K1a) | = *U*(K1a) | = *U*(K1a) | = *U*(K1a) | = *U*(K1a) | = *U*(K1a) |
| K2b | *g* | = 1 − *g*(K1a) | = 1 − *g*(K1a) | = 1 − *g*(K1a) | = 1 − *g*(K1a) | = 1 − *g*(K1a) | = 1 − *g*(K1a) | = 1 − *g*(K1a) | = 1 − *g*(K1a) |
| 16*e* | *x* | −0.0594(2) | −0.1244(7) | −0.1235(6) | −0.1027(6) | −0.1285(11) | −0.102(2) | −0.070(3) | −0.126(2) |
| 32*e*[b] | *y* | = *x* | = *x* | = *x* | = *x* | = *x* | = *x* | = *x* | = *x* |
| | *z* | = *x* | = *x* | = *x* | = *x* | = *x* | = *x* | = *x* | = *x* |
| | *U*/nm$^2$ | = *U*(K1a) | = *U*(K1a) | = *U*(K1a) | = *U*(K1a) | = *U*(K1a) | = *U*(K1a) | = *U*(K1a) | = *U*(K1a) |
| K2c | *g* | | 1 | 1 | 1 | = *g*(K1c) | = *g*(K1c) | = *g*(K1c) | = *g*(K1c) |
| 16*e* | *x* | | 0.4338(4) | 0.4326(4) | 0.4329(4) | 0.432(3) | 0.423(3) | 0.433(2) | 0.4306(7) |
| | y | | = *x* | = *x* | = *x* | = *x* | = *x* | = *x* | = *x* |
| | z | | = *x* | = *x* | = *x* | = *x* | = *x* | = *x* | = *x* |
| | *U*/nm$^2$ | | = *U*(K1a) | = *U*(K1a) | = *U*(K1a) | = *U*(K1a) | = *U*(K1a) | = *U*(K1a) | = *U*(K1a) |
| K2d | *g* | | | | | = 1 − *g*(K1c) | = 1 − *g*(K1c) | | |
| 16*e* | *x* | | | | | 0.4365(10) | 0.4343(9) | | |
| | *y* | | | | | = *x* | = *x* | | |
| | *z* | | | | | = *x* | = *x* | | |
| | *U*/nm$^2$ | | | | | = *U*(K1a) | = *U*(K1a) | | |
| K3a | *g* | 0.055(2) | 0.391(10) | 0.525(6) | 0.562(7) | 0.711(2) | 0.56(2) | 0.56(4) | 0.639(14) |
| 48*h* | *x* | 0.216(2) | 0.2580(14) | 0.2543(10) | 0.2506(8) | 0.2564(8) | 0.249(2) | 0.249(4) | 0.252(2) |
| 96*h*[b] | *y* | 0.263(3) | 0.1201(13) | 0.1320(8) | 0.1210(13) | 0.1221(6) | 0.123(2) | 0.125(3) | 0.120(2) |
| | *z* | 0.1512(11) | 0.1252(14) | 0.1169(7) | 0.1200(14) | 0.1207(7) | 0.121(2) | 0.121(3) | 0.1218(14) |
| | *U*/nm$^2$ | 5.2(3) | 4.3(6) | 4.9(6) | 3.3(5) | 4.2(5) | 0.58(3) | 1.6(6) | 0.8(3) |
| K3b | *g* | | 0.215(12) | 0.310(7) | 0.333(9) | 0.360(9) | 0.33(3) | 0.33(5) | 0.35(2) |
| 48*h* | *x* | | 0.744(3) | 0.742(2) | 0.7280(8) | 0.7598(13) | 0.748(3) | 0.682(3) | 0.750(3) |
| | *y* | | 0.614(2) | 0.6651(9) | 0.6560(8) | 0.6427(7) | 0.6311(13) | 0.672(3) | 0.6308(11) |
| | *z* | | 0.650(2) | 0.6053(10) | 0.6354(7) | 0.6179(7) | 0.6178(13) | 0.614(2) | 0.6164(12) |
| | *U*/nm$^2$ | | = *U*(K3a) | = *U*(K3a) | = *U*(K3a) | = *U*(K3a) | = *U*(K3a) | = *U*(K3a) | = *U*(K3a) |
| K4 | *g* | 0.061(2) | 0.115(6) | 0.221(6) | 0.249(5) | 0.399(10) | 0.254(10) | 0.25(3) | 0.287(12) |
| 16*e* | *x* | 0.128(4) | −0.233(2) | −0.2193(8) | −0.2251(6) | −0.2346(5) | −0.2400(8) | −0.208(3) | −0.2430(9) |
| 96*h*[b] | *y* | 0.124(4) | = *x* | = *x* | = *x* | = *x* | = *x* | = *x* | = *x* |
| | *z* | 0.266(2) | = *x* | = *x* | = *x* | = *x* | = *x* | = *x* | = *x* |
| | *U*/nm$^2$ | 2.2(3) | 4.4(5) | 8.1(5) | 8.4(9) | 5.6(4) | 0.9(4) | 3.8(6) | 2.0(3) |
| K5 | *g* | 0.23(3) | 0.117(7) | 0.932(8) | 0.65(2) | 0.396(8) | 0.72(8) | 0.65(4) | 0.91(2) |
| 24*g* | *x* | 0 | 0.010(14) | −0.0038(12) | −0.007(3) | −0.007(5) | 0.003(2) | −0.002(4) | −0.0003(11) |
| 24*c*[b] | *y* | 1/4 | 1/4 | 1/4 | 1/4 | 1/4 | 1/4 | 1/4 | 1/4 |
| | *z* | 1/4 | 1/4 | 1/4 | 1/4 | 1/4 | 1/4 | 1/4 | 1/4 |
| | *U*/nm$^2$ | = *U*(K4) | = *U*(K4) | = *U*(K4) | = *U*(K4) | = *U*(K4) | = *U*(K4) | = *U*(K4) | = *U*(K4) |
| K6 | *g* | 0.19(4) | 0.42(4) | 0.090(8) | 0.223(6) | 0.330(2) | 0.14(2) | 0.22(3) | 0.09(2) |
| 48*h* | *x* | 0.000(2) | 0.507(3) | 0.504(6) | 0.509(5) | 0.509(3) | 0.519(3) | 0.478(5) | 0.590(4) |
| 96*h*[b] | *y* | 0.225(3) | 0.733(3) | 0.833(7) | 0.749(4) | 0.748(3) | 0.769(3) | 0.770(4) | 0.781(11) |
| | *z* | 0.241(2) | 0.758(2) | 0.841(7) | 0.775(2) | 0.733(2) | 0.758(5) | 0.806(4) | 0.775(12) |
| | *U*/nm$^2$ | = *U*(K4) | = *U*(K4) | = *U*(K4) | = *U*(K4) | = *U*(K4) | = *U*(K4) | = *U*(K4) | = *U*(K4) |

[a] *R* factors attached with primes resulted from MPF. Occupancies for Si1, Si1b, and all O sites are unity, and descriptions of these values are omitted. [b] Note: Multiplicities plus Wyckoff letters with and without *b* are those for space groups $F\bar{4}3c$ and *F*23, respectively.

were also detected in optical absorption and ESR spectra.[2,51] Cationic Na clusters showing diamagnetism are formed in $\beta$-cages of Na-LTA.[5] The kind and number of alkali metal ions in cages of LTA doped with alkali metals strongly affect the atomic configuration of the clusters and, consequently, their physical properties.

Optical spectra provided no evidence for the existence of K clusters in the $\beta$-cage of $K_n$/K-LTA.[2] Woodall et al.[46] did not detect any paramagnetic signal with hyperfine structures in an ESR spectrum of $K_{0.5}$/K-LTA. We also observed no hyperfine structures in the ESR spectrum of $K_{0.01}$/K-LTA, where K clusters are sufficiently far together to act as localized paramagnetic species. These experimental facts suggest that guest 4s electrons are confined not in the $\beta$-cages but in the $\alpha$-cages. If 4s electrons were included in the $\beta$-cages, they would completely be isolated to exhibit paramagnetism with hyperfine structures observed in the ESR spectrum and a photoabsorption band at 2.5−3.0 eV.[2,51,52]

$K^+$ ions in the $\beta$-cage of $K_{0.35}$/K-LTA form a regular octahedron and/or a regular tetrahedron in our $F\bar{4}3c$ model. On the other hand, no K clusters such as $K_3^{2+}$ and $K_4^{3+}$ exist in $K_n$/K-LTA with $n > 0.35$, because hardly any localized electron densities were detected between $K^+$ ions in the $\beta$-cage (Figure 5). Paramagnetic K clusters (e.g., $K_3^{2+}$ [47]) are regarded not as a major chemical species but as a minor one, because a simple resonating signal contributes for the most part to the ESR[46]

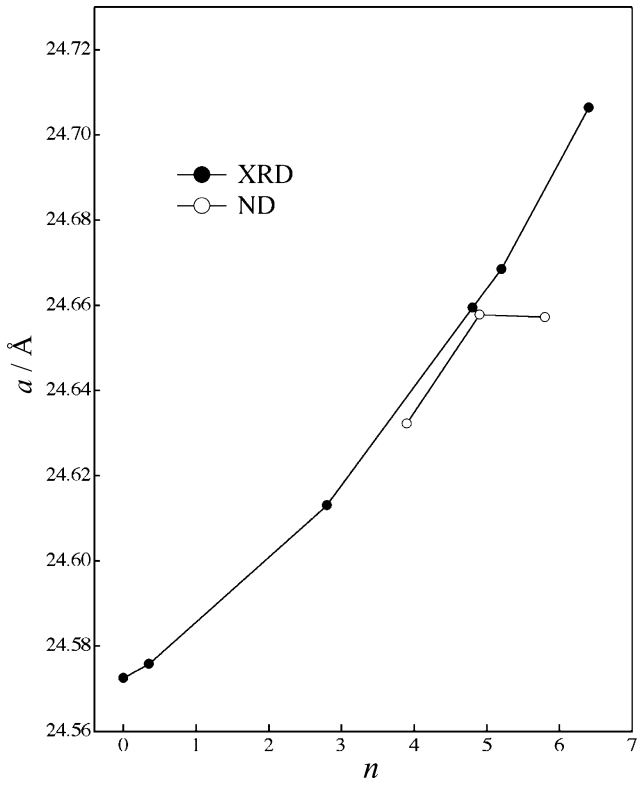


**Figure 3.** Dependence of the lattice parameter $a$ on $n$ in $K_n$/K-LTA at room temperature (XRD) and the low temperatures (ND).

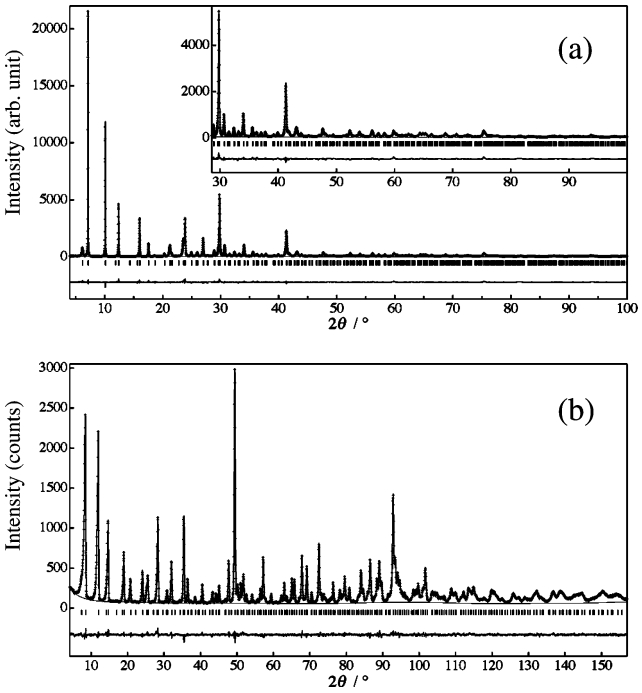


**Figure 4.** Observed, calculated, and difference patterns for MPF of (part a) the XRD data for $K_{6.4}$/K-LTA and (part b) the ND data for $K_{5.8}$/K-LTA at 7 K.

spectrum. Then, we will focus attention on 4s electrons affording simple ESR signals and K clusters which include 4s electrons.

$K^+$ ions will occupy positions with $l$(K−K) near 4.54 Å, which is the shortest distance between K atoms in metallic potassium, to reduce the total electrostatic potential in the $\beta$-cage as much as possible. The K sites in the $\beta$-cage approach the α-cage with decreasing temperature. The shortest K1a−K1a and K2c−K2c distances at room temperature are 4.47(4) and 4.68-

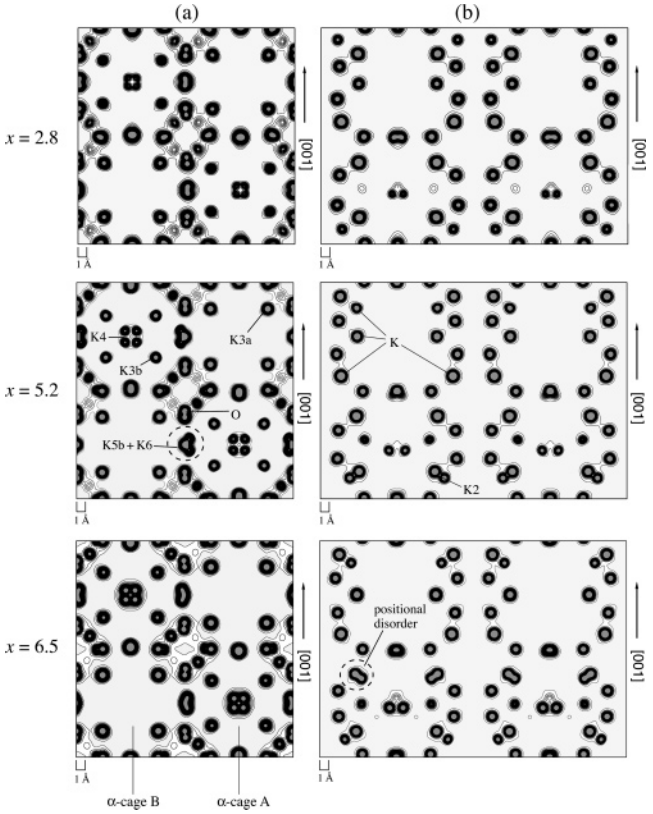


**Figure 5.** Electron density distribution in $K_n$/K-LTA ($n$ = 2.8, 5.2, and 6.5). Electron densities were summed up in a $z$ range of $0.21 < z < 0.29$ parallel to the $c$ axis and projected onto (part a) the (001) plane and (part b) the (110) plane. Contour lines were plotted for (part a) 5−120 e/Å$^3$ with a step of 3 e/Å$^3$ and (part b) 0.3−10 e/Å$^3$ with a step of 0.4 e/Å$^3$.

(3) Å, respectively (Table 2). These distances, which seem to be reasonable considering the $l$(K−K) value in metallic potassium, were found to be proportional to the $g$(K) values of the K sites in the $\beta$-cage. The local atomic arrangement of four K1a atoms in the $\beta$-cage is far from the regular tetrahedron, as shown by $g$(K1a) as low as 0.616.

Electron densities of K atoms near the six-membered ring were rather high. The oxidation state of these K atoms is regarded as +1 in view of the distance, $l$(K−O) ≈ 3.1 Å, between K and O atoms in the six-membered ring; this value is typical of K−O bond lengths in zeolites. Electron densities due to chemical bonding are clearly visible between $K^+$ ions and O atoms in the electron density maps obtained by MPF in all the samples of $K_n$/K-LTA. $K^+$ ions near the six-membered ring are, therefore, strongly attracted toward the nearest oxygen atoms in the framework.

**C. Atomic Arrangement of K Clusters in the α-Cage.** In the $F23$ model, α-cages A and B are nonequivalent to each other. The framework was distorted to a greater extent with increasing $n$, which results in slightly different volumes of α-cages A and B. The distortion is caused by the static displacements of sites O3 and O4 in α-cage B and sites O3b and O4b in α-cage A.

K atoms have properties intermediate between ionic and metallic ones in view of interatomic distances between each K atom and its neighboring atoms. In the α-cage, $l$(K−K) values, except $l$(K5−K6) relevant to the split K5 and K6 sites, range widely from 2.9 o 5.5 Å with an average distance of 4.3 Å. The minimum $l$(K−K) is ca. 2.94 Å, which is about twice as large as the effective ionic radius (1.37 Å) of the $K^+$ ion in

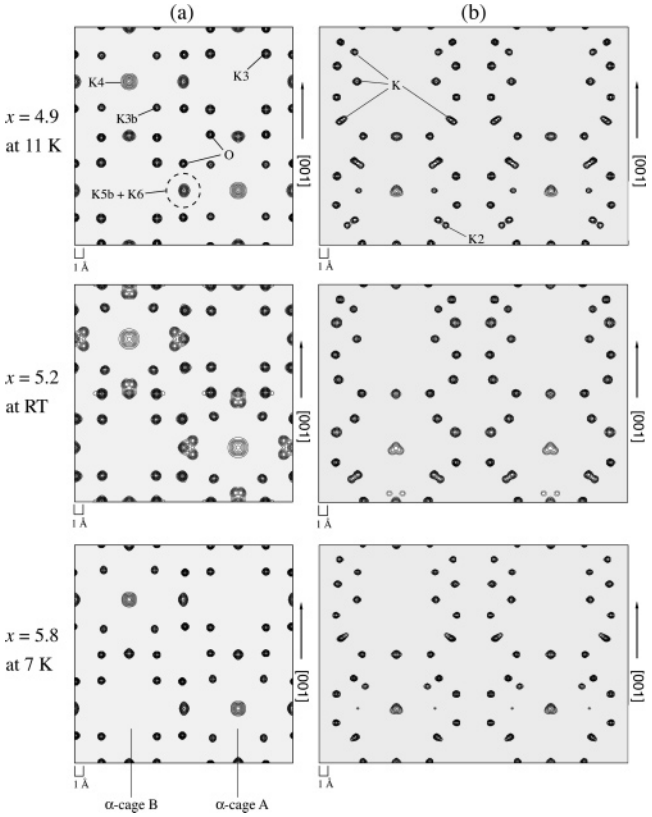


**Figure 6.** Nuclear density distribution in $K_n$/K-LTA ($n = 4.9$ at 11 K, $n = 5.2$ at 300 K, and $n = 5.8$ at 7 K). Nuclear densities were summed up in a $z$ range of $0.21 < z < 0.29$ parallel to the $c$ axis and projected onto (part a) the (001) plane and (part b) the (110) plane. Contour lines were plotted for (part a) $0.3 \times 2.1^N$ fm/Å$^3$ with $N = 1-10$ and (part b) $0.3 \times 2.1^N$ fm/Å$^3$ with $N = 1-9$.

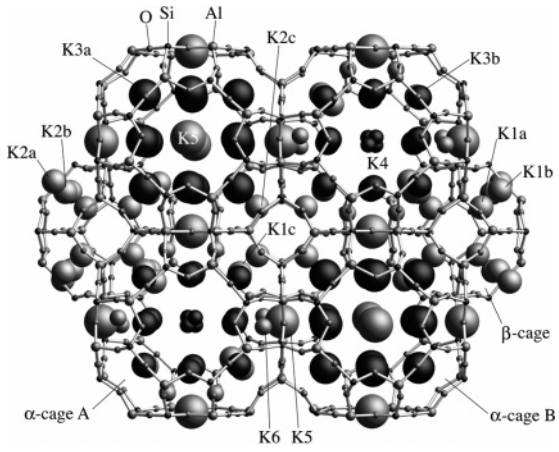


**Figure 7.** Structure of $K_{5.2}$/K-LTA viewed along the [100] direction.

4-fold coordination.[53] Accordingly, K−K bonds shorter than 4.54 Å are probable between K atoms of highly ionic character.

Occupancies of site K3a in α-cage B and sites K3b and K4 in α-cage A increase with an increase in $n$. In the samples with $n > 0.35$, $g$(K3a) − $g$(K3b) reached a maximum in $K_{6.4}$/K-LTA: $g$(K3a) = 0.711(2) and $g$(K3b) = 0.360(9). In dehydrated K-LTA, these two sites close to the four-membered ring are scarcely occupied because of higher potential energies at these positions in comparison with the other cation sites near the six- and eight-membered rings. Nevertheless, $g$(K3a) and $g$(K3b) considerably increased with increasing $n$ from 2.8 to 6.4, ranging from 0.391(10) to 0.711(2) and from 0.215(12) to 0.360(9), respectively. This fact offers unambiguous evidence that no K clusters with definite numbers of K atoms are formed in α-cage A or B. For example, the existence of a $K_{12}^{4+}$ cluster claimed by Armstrong et al.[22] would require full occupation of site K3a or K3b. The $g$(K4) value also increased with increasing $n$, ranging from 0.115(6) to 0.399(10).

Nuclear density maps evidenced a disordered distribution of K atoms near the center of the six-membered ring. Nuclear densities near site K4 were rather dispersed. Site K5 lies beside the center of the eight-membered ring, and site K6 is close to site K5. The very short K5−K6 distance of ca. 1.0 Å implies that either K5 or K6 is locally included in the eight-membered ring without any ordering. K6 approaches K5 with a decrease in temperature. The total number of $K^+$ ions calculated from $g$(K5) and $g$(K6) was roughly equal to unity per eight-membered ring.

The K clusters in the α-cages are regarded as metastable, because the clusters are supported by the framework. The local symmetry of each K cluster must be lower than that of the average disordered structure based on space groups $F\bar{4}3c$ and $F23$. The local symmetry seems to affect the configuration of electron spins in the K cluster as will be described in the next section.

**D. Magnetic Ordering of $K_n$/K-LTA.** The presence of the nonequivalent K clusters in α-cages A and B in our crystal data provides us with a clue to the elucidation of the magnetism in the present system. Differences between the numbers of $K^+$ ions between the K clusters in α-cages A and B is denoted as $\Delta N$, hereafter. Figure 8 shows both magnetization (cited from ref 3) and $\Delta N$, which strongly depend on the K atom loading density, $n$. Dehydrated and $K_{0.35}$/K-LTA samples show no ferromagnetism and $\Delta N = 0$, derived from equivalent K positions in adjacent α-cages. In the ferromagnetic samples with $2.8 \leq n \leq 5.2$, the difference in the number of $K^+$ ions, $\Delta N$, was estimated to be 1.7−1.8 from $g$(K3a), $g$(K3b), and $g$(K4) (Table 3), and the spontaneous magnetization increased with increasing $n$. In the region $n > 5.2$, $\Delta N$ increased with increasing $n$; nevertheless, the spontaneous magnetization decreased. $\Delta N$ is approximately equal to a difference in the number of 4s electrons between the K clusters in α-cages A and B. The dependence of $\Delta N$ on $n$ provides significant information regarding the magnetism in $K_n$/K-LTA.

It has been made clear that the electronic levels for the 4s electrons in the K clusters can be approximately described starting from a model of a spherical quantum well.[2,54] Loaded 4s electrons in the α-cage occupy 1s,1p cluster orbitals in this model. On the appearance of ferromagnetism, the occupation of the 4s electrons on the 1p orbital is significantly important. In other words, the total number of K atoms loaded into the α-cage is more than two, on the average, for the appearance of ferromagnetism. In the spherical potential model, the 1p orbital is triply degenerated. Considering the spin degeneracy, six electrons can occupy the 1p orbitals. Two, three, and four 4s electrons occupying the triply degenerated 1p orbitals can have high spin states (viz., $S = 1$, 3/2, and 1) originating from the Hund coupling. However, the symmetry of the actual potential inside the α-cage is not spherical. 1p orbitals will split depending on the local symmetry. The local symmetry in the α-cage seems to strongly depend on the actual occupation of $K^+$ ions in an α-cage. Total occupancies of K sites near the six- and eight-membered rings are close to unity and independent of the amount of loaded K atoms as already described. Therefore, these sites will have a small contribution on the splitting of the degenerated 1p orbitals. In contrast, the occupancies of $K^+$ ions close to the four-membered ring (i.e., K3a and K3b sites) are not unity, and the occupancy of these sites increases with

**TABLE 2: Interatomic Distances, *l*'s, and Bond Angles, $\phi$'s, Obtained for $K_{5.2}$/K-LTA by XRD[a]**

| | *l*/Å | | *l*/Å | | $\phi$/° |
|---|---|---|---|---|---|
| Si1−O1 | 1.77(4) | K3b−O1$^{vi}$ | 3.91(6) | O1−Si1−O2 | 106(2) |
| Si1−O2 | 1.70(6) | K3b−O1b | 3.48(6) | O1−Si1−O3b$^{i}$ | 107(2) |
| Si1−O3b$^{i}$ | 1.60(5) | K3b−O3b | 3.74(3) | O1−Si1−O4$^{ii}$ | 104(2) |
| Si1−O4$^{ii}$ | 1.74(5) | K3b−O4b | 3.14(3) | O2−Si1−O3b$^{i}$ | 113(2) |
| Al, Si2−O1b$^{iii}$ | 1.75(4) | K5−O1 | 3.19(4) | O2−Si1−O4$^{ii}$ | 108(2) |
| Al, Si2−O2 | 1.73(6) | K5−O1b$^{ix}$ | 3.22(4) | O3b$^{i}$−Si1−O4$^{ii}$ | 117(2) |
| Al, Si2−O3b$^{iv}$ | 1.63(5) | K5−O2 | 3.66(2) | O1b−Si1b−O2b | 109(2) |
| Al, Si2−O4 | 1.77(6) | K5−O2b$^{ix}$ | 3.93(2) | O1b−Si1b−O3$^{v}$ | 121(3) |
| Si1b−O1b | 1.54(4) | K6−O1$^{i}$ | 3.24(9) | O1b−Si1b−O4b | 102(2) |
| Si1b−O2b | 1.58(5) | K6−O1b$^{v}$ | 2.61(6) | O2b−Si1b−O3$^{v}$ | 98(2) |
| Si1b−O3$^{v}$ | 1.71(4) | K6−O2$^{i}$ | 3.23(8) | O2b−Si1b−O4b | 103(2) |
| Si1b−O4b | 1.60(5) | K6−O2b$^{v}$ | 3.53(7) | O3−Si1b−O4b | 120(2) |
| Alb, Si2b−O1$^{vi}$ | 1.75(5) | K1a−K1a | 4.47(4) | O1b−Al1−O2 | 109(2) |
| Alb, Si2b−O2b | 1.66(5) | K1a−K2b | 4.33(2) | O1b−Al1−O3b$^{vii}$ | 107(3) |
| Alb, Si2b−O3$^{vii}$ | 1.65(4) | K1a−K1b | 2.34(4) | O1b−Al1−O4 | 112(2) |
| Alb, Si2b−O4b | 1.84(6) | K1c−K3b | 2.93(2) | O2−Al1−O3b$^{vii}$ | 104(2) |
| K1a−O2 | 3.33(2) | K2a−K3b | 3.56(2) | O2−Al1−O4 | 108(2) |
| K1a−O4$^{ii}$ | 2.81(2) | K2a−K2b | 1.17(3) | O3b−Al1−O4 | 116(2) |
| K1b−O2 | 3.24(2) | K2c−K2c$^{v}$ | 4.68(3) | O1$^{iv}$−Al2−O2b | 109(2) |
| K1b−O4$^{ii}$ | 2.57(3) | K3a−K3a | 4.50(3) | O1$^{iv}$−Al2−O3$^{iii}$ | 121(2) |
| K1c−O2b | 2.87(2) | K3b−K3b | 2.94(3) | O1$^{iv}$−Al2−O4b$^{viii}$ | 95(2) |
| K1c−O4b | 2.60(2) | K3b−K3b$^{xv}$ | 4.45(3) | O2b−Al2−O3$^{iii}$ | 108(2) |
| K2a−O2 | 3.07(2) | K5−K6 | 0.62(5) | O2b−Al2−O4b$^{viii}$ | 104(2) |
| K2a−O3b$^{xii}$ | 1.84(6) | K5−K1b | 5.53(4) | O3$^{iii}$−Al2−O4b$^{viii}$ | 118(2) |
| K2b−O2 | 2.78(2) | K5−K1c$^{ix}$ | 5.36(4) | Si1−O1−Al2, Si2b$^{ix}$ | 132(2) |
| K2b−O3b$^{xii}$ | 2.62(2) | K5−K2a | 5.17(4) | Si1−O2−Al1, Si2 | 168(2) |
| K2c−O3$^{vii}$ | 2.40(2) | K5−K3a | 4.47(7) | Si1b$^{v}$−O3−Al2, Si2b$^{x}$ | 138(1) |
| K2c−O2b$^{vii}$ | 2.60(2) | K6−K3b$^{v}$ | 3.60(9) | Si1−O4−Al1, Si2 | 143(1) |
| K3a−O1 | 2.96(7) | | | Si1b−O1b−Al1, Si2$^{i}$ | 129(3) |
| K3a−O1b$^{xiii}$ | 2.95(7) | | | Si1b−O2b−Al2, Si2b | 169(2) |
| K3a−O3$^{xiv}$ | 3.12(3) | | | Si1$^{i}$−O3b−Al1, Si2$^{i}$ | 155(2) |
| K3a−O4$^{xiv}$ | 2.82(3) | | | Si1b$^{ii}$−O4b−Al2, Si2b$^{ii}$ | 142(2) |

[a] Symmetry codes: (*i*) 1/2 + *y*,1/2 − *z*, −*x*; (*ii*) *y*, 1/2 + *z*, 1/2 + *x*; (*iii*) *x*, 1/2 − *y*, 1.2 − *z*; (*iv*) *y*, 1/2 − *z*, 1.2 − *x*; (*v*) −*x*, 1/2 + *y*, 1/2 − *z*; (*vi*) 1/2 + *x*, *y*, 1/2 + *z*; (*vii*) 1/2 + *y*, −*z*, 1/2 − *x*; (*viii*) 1/2 + *x*, 1/2 − *y*, −*z*; (*ix*) 1/2 + *z*, 1/2 + *x*, *y*; (*x*) −*x*, *y*, −*z*; (*xi*) 1/2 + *y*, 1/2 − *z*, *x*; (*xii*) *x*, 1/2 + *y*, 1/2 + *z*; (*xiii*) 1/2 + *z*, *x*, 1/2 + *y*; (*xiv*) *z*, 1/2 − *x*, 1/2 − *y*; (*xv*) 1/2 − *x*, 1/2 + *y*, −*z*.

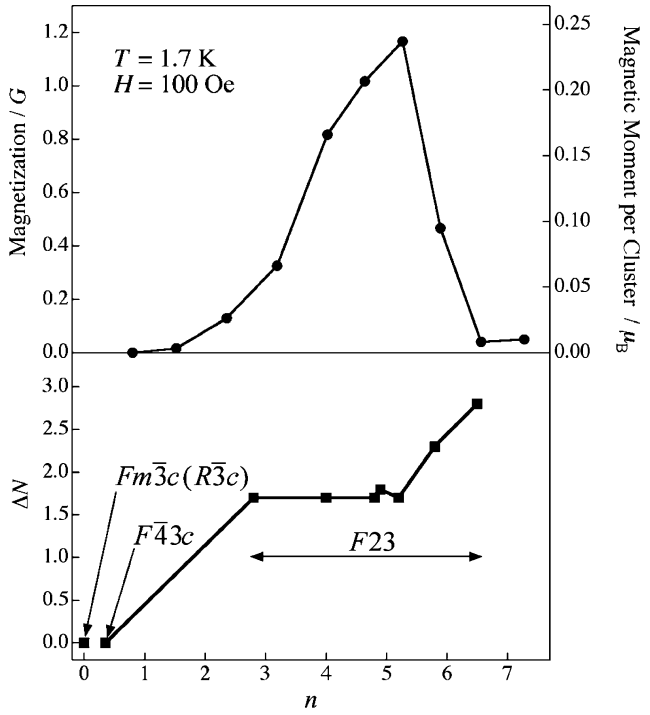


**Figure 8.** Dependence of the magnetic moments/magnetization (upper side) in ref 3 and $\Delta N$ value (lower side) on *n* in $K_n$/K-LTA derived from all diffraction data. Space groups at each *n* value are denoted.

increasing K loading density. Thus, the actual occupation of these sites will lower the local potential from the cubic symmetry, which will split the 1p orbitals. Because of the splitting, the 4s electrons in the 1p orbitals of the K cluster may not have high spin states or may have $S = 0$.

**TABLE 3: Differences, $\Delta N$'s, in the Number of $K^+$ Ions between K Clusters in α-cages A and B, and Total Numbers of $K^+$ Ions near the Center of the Eight-Membered Ring, *n*(8-MR), in $K_n$/K-LTA[a]**

| | XRD | | | |
|---|---|---|---|---|
| | α-cage *A* | α-cage *B* | $\Delta N = (A - B)$ | *n*(8-MR) |
| $K_{2.8}$ @ K-LTA | 4.7 | 3.0 | 1.7 | 2.8 |
| $K_{4.8}$ @ K-LTA | 6.3 | 4.6 | 1.7 | 3.3 |
| $K_{5.2}$ @ K-LTA | 6.7 | 5.0 | 1.7 | 3.3 |
| $K_{6.5}$ @ K-LTA | 8.9 | 6.1 | 2.8 | 3.1 |
| | ND | | | |
| | α-cage *A* | α-cage *B* | $\Delta N = (A - B)$ | *n*(8-MR) |
| $K_{4.0}$ @ K-LTA[b] | 5.8 | 4.0 | 1.7 | 3.1 |
| $K_{4.9}$ @ K-LTA | 6.7 | 4.9 | 1.8 | 3.0 |
| $K_{5.8}$ @ K-LTA | 7.7 | 5.4 | 2.3 | 3.3 |

[a] Determined from the XRD data at room temperature and the ND data at low temperature. [b] Obtained by the Rietveld analyses of the TOF ND data.[25]

From the analysis of $^{29}$Si NMR spectra, Kira et al.[20] claimed that magnetic moments had spin quantum numbers of $S = 1$ and $S = 0$ for the neighboring α-cages. We have to consider that they measured the NMR spectra under a magnetic field of 3.93 T for loaded K atoms of $n = 4-7$. The spontaneous magnetization of the $K_n$/K-LTA which shows ferromagnetism is very sensitive to the external magnetic field.[3,13] The NMR measurements seem to not be observing the actual ferromagnetic state and electron spin state at external zero magnetic field. Anyway, for a wide range of the K loading densities, to satisfy the spin quantum numbers of $S = 1$ and 0 which they proposed for the K clusters in the two adjacent α-cages, 4s electrons with an even number have to occupy α-cages A and B. The 1p orbital has to be doubly degenerated at the K cluster with $S = 1$. For

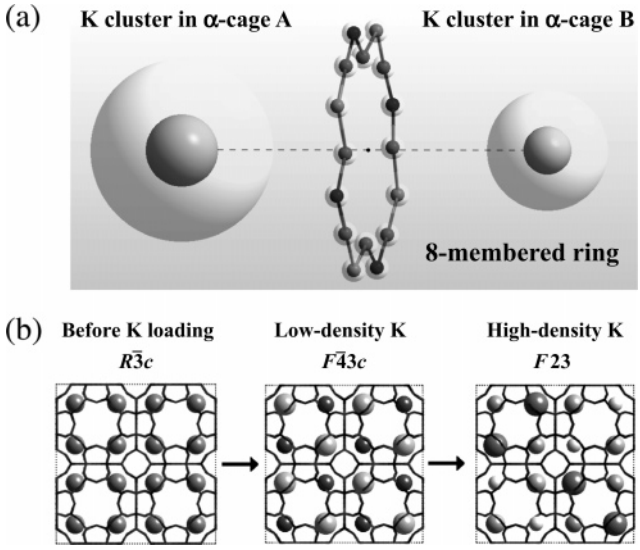


**Figure 9.** (part a) Nonequivalent K clusters in α-cages A and B. The middle point between the two clusters lies at the center of the eight-membered ring. (part b) Changes in the local symmetry of the K clusters with increasing *n*.

example, the configuration of 4s electrons in the two α-cages A and B at $n = 3$, 4, and 5 can be described as $1s^2$ and $1s^21p^2$, $1s^2$ and $1s^21p^4$, and $1s^21p^4$ and $1s^21p$,[6] respectively. At $n = 4$, it is also possible to have a configuration of $1s^21p^2$ in both α-cages, where one of the α-cages should have a nondegenerated 1p orbital occupied by two 4s electrons and the other should have a degenerated 1p orbital occupied by two 4s electrons. The difference between the electrons in the two α-cages has the largest or smallest value of four or zero at $n = 4$. Their model seems to be, accordingly, incompatible with the constant and monotonic increase in $\Delta N$ with increasing *n*.

Nakano et al. proposed a model in which a localized spin of $S = 1/2$ (i.e., odd numbers of 4s electrons) distributes in each α-cage.[15] In their model, if the average loading density *n* is an odd number, then α-cages A and B will both have the same number of electrons, *n*. If *n* is close to even, α-cages A and B should have different numbers of electrons. For example, the numbers of electrons are $n + 1$ and $n - 1$ for α-cages A and B, respectively. This means that the difference in the number of 4s electrons between adjacent α-cages A and B changes from zero to two depending on the *n*.

In the present, we cannot definitely determine from a viewpoint of crystallography which model is adequate. The interaction between the K clusters in adjacent α-cages may be not negligible for the difference of electron numbers of the neighboring α-cages. Further detailed measurements of the electronic properties are necessary. For example, the muon spin rotation/relaxation ($\mu$SR) study[55] for a wide range of *n* values will be very important, because it gives us information of the internal field distribution in the magnetically ordered state.

The finite DM interaction requires the absence of an inversion center at the middle point between two magnetic moments.[16−18] In the present system, the middle point between the K clusters in α-cages A and B corresponds to the center of the eight-membered ring (Figure 9a), where no inversion center exists in favor of the DM interaction. Figure 9b schematically illustrates changes in the arrangements of K atoms with increasing *n*. Space groups $Fm\bar{3}c$, $F\bar{4}3c$, and $F23$, where site symmetries at the center of the eight-membered ring are, respectively, $4/m..$, $\bar{4}..$, and 2.., satisfy the prerequisite for the DM interaction. The lowering of space group symmetry from $Fm\bar{3}c$ to $F23$ by increasing *n* changes the point group symmetries of the K1 and K2 sites near the six-membered ring from $O_h$ to $T$ and the arrangement of K atoms in α-cages A and B from equivalent to nonequivalent. We, therefore, propose a magnetic ordering model introducing the spin-canting mechanism. The magnetic moments of the K clusters in adjacent α-cages are not completely ordered in an antiparallel way but are slightly tilted toward the [100] direction, so that the finite macroscopic magnetization is induced. The actual easy axis of magnetization remains unknown at present.

As described previously, the increases in $\Delta N$ between α-cages A and B (Table 3) with increasing *n* in the region of $n \geq 5.2$ give rise to two kinds of physical behavior. First, the spin-canting effect originating from the DM interaction increases with increasing *n*. Second, increasing $\Delta n$ in the region of $n \geq 5.2$ increases a difference in energy level between the discrete electronic states of the neighboring K clusters. Hence, $T_C$ and $T_W$, which respectively reach the maximum and minimum values at $n \approx 4$, eventually approach 0 K (paramagnetic behavior) with increasing *n* even if the DM interaction is enhanced.

## 5. Summary

Crystal structures of K-doped zeolite K-LTA with wide range control on the K loading densities are determined from XRD and ND data, which have equivalent $K^+$ ions arrangements in adjacent α-cages with space groups $F\bar{4}3c$ at $n = 0.35$ and nonequivalent ones with space group $F23$ in an *n* region of $n \geq 2.8$. In fact, crystal symmetry is degraded with increasing *n*. From our crystal structures determined in this study, we conclude that the dependence of $\Delta N$ on *n* is strongly concerned with the behavior of magnetization and the different distribution of the $K^+$ ions in α-cages A and B is indispensable for the spin-canting model arising from the DM interaction among K clusters in this ferromagnetic phenomenon.

In the future, we should investigate the irregular conformation of each K cluster associated with the lowering of the local symmetry of K clusters with the disordered arrangement of K atoms. The local structures of the K clusters including 4s electrons must strongly influence local magnetic interactions. Neutron powder diffraction experiments with an intense neutron source would also serve to verify the validity of the spin-canting model from magnetic scattering data.

**Acknowledgment.** We thank Y. Nozue, T. Nakano, and Y. Ikemoto for fruitful discussions and comments. Thanks are also due to S. Kumazawa for his help in the development the MPF method.

## References and Notes

(1) Nozue, Y.; Kodaira, T.; Goto, T. *Phys. Rev. Lett.* **1992**, *68*, 3789−3792.

(2) Kodaira, T.; Nozue, Y.; Ohwashi, S.; Goto, T.; Terasaki, O. *Phys. Rev. B* **1993**, *48* , 12245−12252.

(3) Nozue, Y.; Kodaira, T.; Ohwashi, S.; Goto, T.; Terasaki, O. *Phys. Rev. B* **1993**, *48* , 12253−12261.

(4) Srdanov, V. I.; Stucky, G. D.; Lippmaa, E.; Engelhardt, G. *Phys. Rev. Lett.* **1998**, *80*, 2449−2452.

(5) Kasai, P. H. *J. Chem. Phys.* **1965**, *43*, 3322−3227.

(6) Kodaira, T.; Takeo, H.; Nozue, Y. *Proceedings Science and Technology of Atomically Engineered Materials*. World Scientific: Singapore, 1996; pp 85−90.

(7) Nozue, Y.; Ikemoto, Y.; Nakano, T.; Terasaki, O.; Kodaira, T.; Takeo, H. *Mater. Res. Soc. Jpn.* **1996**, *20*, 458−461.

(8) Armstrong, A. R.; Anderson, P. A.; Woodall, L. J.; Edwards, P. P. *J. Phys. Chem.* **1994**, *98*, 9279−9284.

(9) Nozue, Y.; Kodaira, T.; Ohwashi, S.; Goto, T.; Terasaki, O. *Surf. Rev. Lett.* **1996**, *3*, 701−706.

(10) Nakano, T.; Ikemoto, Y.; Nozue, Y. *J. Magn. Magn. Mater*. **2001**, *226*−*230*, 238−240.
(11) Madsen, G. K. H.; Gatti, C.; Iversen, B. B.; Damjanovic, L.; Stucky, G. D.; Srdanov, V. I. *Phys. Rev. B* **1999**, *59*, 12359−12369.
(12) Loewenstein, W. *Am. Mineral*. **1954**, *39*, 92−96.
(13) Nakano, T.; Ikemoto, Y.; Nozue, Y. *Eur. Phys. J. D.* **1999**, *9*, 505−508.
(14) Ikemoto, Y.; Nakano, T.; Nozue, Y.; Terasaki, O.; Qiu, S. *Mater. Sci. Eng.* **1997**, *B48*, 116−121.
(15) Nakano, T.; Ikemoto, Y.; Nozue, Y. *Physica B* **2000**, *281*−*282*, 688−690.
(16) Dzyaloshinsky, I. *J. Phys. Chem. Solids* **1958**, *4*, 241−255.
(17) Moriya, T. *Phys. Rev. Lett*. **1960**, *4*, 228−230.
(18) Moriya, T. *Phys. Rev.* **1960**, *120*, 91−98.
(19) Maniwa, Y.; Kira, H.; Shimizu, F.; Murakami, Y. *J. Phys. Soc. Jpn*. **1999**, *68*, 2902−2905.
(20) Kira, H.; Tou, H.; Maniwa, Y.; Murakami, Y. *Physica B* **2001**, *312*−*313*, 789−790.
(21) Tao, S.; Seff, K. *J. Phys. Chem*. **1993**, *97*, 10756−10760.
(22) Armstrong, A. R.; Anderson, P. A.; Edwards, P. P. *J. Solid State Chem*. **1994**, *111*, 178−184.
(23) Nishibori, E.; Nakamura, K.; Tsukamoto, M.; Takata, M.; Sakata, M.; Shimizu, F.; Kira, H.; Maniwa, Y. *Abstracts 3rd Workshop of the Research Group on Ultrafine Particles and Clusters*; 1999; pp 181−184.
(24) Ikeda, T.; Kodaira, T.; Izumi, F.; Kumazawa, S. *Mol. Cryst. Liq. Cryst*. **2000**, *341*, 447−452.
(25) Ikeda, T.; Kodaira, T.; Izumi, F.; Kamiyama, T. *Chem. Phys. Lett*. **1999**, *318*, 93−101.
(26) Collins, D. M. *Nature* **1982**, *298*, 49−51.
(27) Sakata, M.; Sato, M. *Acta Crystallogr*. **1990**, *A46*, 263−270.
(28) Izumi, F.; Ikeda, T. *Mater. Sci. Forum* **2000**, *321*−*324*, 198−203.
(29) Izumi, F.; Kumazawa, S.; Ikeda, T.; Ida, T. *Powder Diffraction*; Sen Gupta, S. P. Ed.; Allied Publishing: New Delhi, 1998; Chapter 2, pp 24−36.
(30) Izumi, F.; Kumazawa, S.; Ikeda, T.; Hu, W.-Z.; Yamamoto, A.; Oikawa, K. *Mater. Sci. Forum* **2001**, *378*−*381*, 59−64.
(31) Ikeda, T.; Izumi, F.; Kodaira, T.; Kamiyama, T. *Chem. Mater*. **1998**, *10*, 3996−4004.
(32) *Inorganic Synthesis*; Holt, S. L., Jr., Ed.; Wiley: New York, 1983; Vol. 22, pp 61−68.
(33) Pluth, J. J.; Smith, J. V. *J. Phys. Chem*. **1979**, *83*, 741−749.
(34) Adams, J. M.; Haselden, D. A.; Hewat, A. W. *J. Solid State Chem.* **1982**, *44*, 245−253.
(35) Rayment, T.; Thomas, J. M. *Zeolites* **1983**, *3*, 2−4.
(36) *International Tables for Crystallography*, 2nd ed.; Wilson, A. J. C., Prince, E., Eds.; Kluwer: Dordrecht, The Netherlands, 1999; Vol. C, pp. 441−448 and pp 572−574.
(37) Tokonami, M. *Acta Crystallogr*. **1965**, *19*, 486.
(38) Toraya, H. *J. Appl. Crystallogr*. **1990**, *23*, 485−491.
(39) Ohta, T.; Izumi, F.; Oikawa, K.; Kamiyama, T. *Physica B* **1997**, *234*, 1093−1095.
(40) Rietveld, H. M. *J. Appl. Crystallogr*. **1969**, *2*, 65−71.
(41) Kumazawa, S.; Kubota, Y.; Takata, M.; Ishibasi, Y. *J. Appl. Crystallogr*. **1993**, *26*, 453−457.
(42) Knorr, K.; Madler, F.; Papoular, R. J. *Microporous Mesoporous Mater*. **1998**, *21*, 353−363.
(43) Takata, M.; Nishibori, E.; Sakata, M. *Z. Kristallogr*. **2001**, *216*, 71−86.
(44) Papoular, R. J.; Cox, D. E. *Europhys. Lett*. **1995**, *32*, 337−342.
(45) Adams, J. M.; Haselden, D. A. *J. Solid State Chem*. **1983**, *47*, 123−131.
(46) Woodall, L. J.; Anderson, P. A.; Armstrong, A. R.; Edwards, P. P. *J. Chem. Soc., Dalton Trans*. **1996**, 719−727.
(47) Edwards, P. P.; Anderson, P. A.; Thomas, J. M. *Acc. Chem. Res*. **1996**, *29*, 23−29.
(48) Harrison, M. R.; Edwards, P. P.; Klinowski, J.; Thomas, J. M.; Johnson, D. C.; Page, J. *J. Solid State Chem*. **1984**, *54*, 330−341.
(49) Ursenbach, C. P.; Madden, P. A.; Stich, I.; Payne, M. C. *J. Phys. Chem*. **1995**, *99*, 6697−6714.
(50) Ikemoto, Y.; Nakano, T.; Kuno, M.; Nozue, Y.; Ikeda, T. *J. Magn. Magn. Mater*. **2001**, *226*−*230*, 229−232.
(51) Kodaira, T.; Nozue, Y.; Goto, T. *Mol. Cryst. Liq. Cryst*. **1992**, *218*, 55−60.
(52) Oh, T.; Yu, J. S.; Ikeda, T.; Kodaira, T. *Solid State Commun*. **2002**, *123*, 387−390.
(53) Shannon, R. D. *Acta Crystallogr*. **1976**, *A32*, 751−767.
(54) Nakano, T.; Ikemoto, Y.; Nozue, Y. *J. Phys. Soc. Jpn*. **2002**, *71*, 199−201.
(55) Nakano, T.; Kiniwa, D.; Platt, F. L.; Watanabe, I.; Ikemoto, Y.; Nozue, Y. *Physica B* **2003**, 326, 550−555.